# Automatic tuning of MST segmentation of mammograms for registration and mass detection algorithms

Mariusz Bajger, Fei Ma, Murk J. Bottema
School of Computer Science, Engineering and Mathematics
Flinders University, Adelaide, SA 5001, Australia
{mbajger, ma029, murkb}@csem.flinders.edu.au

## Abstract

*A technique utilizing an entropy measure is developed for automatically tuning the segmentation of screening mammograms by minimum spanning trees (MST). The lack of such technique has been a major obstacle in previous work to segment mammograms for registration and applying mass detection algorithms. The proposed method is tested on two sets of mammograms: a set of 55 mammograms chosen from a publicly available Mini-MIAS database, and a set of 37 mammograms selected from a local database. The method performance is evaluated in conjunction with three different preprocessing filters: gaussian, anisotropic and neutrosophic. Results show that the automatic tuning has the potential to produce state-of-the art segmentation of mass-like objects in mammograms. The neutrosophic filtering provided the best performance.*

## 1 Introduction

Anomalies in mammograms associated with cancer, especially those associated with early cancer, often resemble normal tissue patterns. This complicates the interpretation of mammograms for computer-aided diagnostic (CAD) schemes as well as human readers. The static resemblance between normal and diseased tissue may be mitigated through bilateral comparison or, when available, temporal comparison. Human observers are often able to perform such comparisons very well, but computer algorithms for this task are problematic. Central to CAD comparison of mammograms is image registration. In order to decide if there are new anomalies, evidence of changes in appearance of anomalies, or if patterns between the left and right breast are different, algorithms must have the ability to associate objects between images. The registration process is increasingly important for the detection of pathologies at early stages [10].

Two general classes of image registration techniques are local matching of pixel intensity values and the use of landmarks. Many registration schemes use a combination of both these approaches. However, neither of these techniques are particularly well suited for registration of mammograms. The matching of local pixel intensities is compromised by the fact that the same object in two views of the same breast may be represented by very different sets of intensity values. This is due, in turn, to the contortion of breast tissue during image acquisition, differences in exposure and positioning as well as normal changes of surrounding breast tissue over time. Landmarks in mammograms may include the border of the pectoral muscle, the nipple, and the breast boundary [10]. The nipple is often difficult to detect and the breast boundary is not entirely invariant between different images of the same breast due to the inconsistencies of image acquisition mentioned above. The pectoral muscle boundary does not change substantially over time, is not subject to distortion at acquisition and is usually easy to delineate near the top of medio lateral views. However, the boundary tends to fade below the middle of the image and is absent in cranial caudal views. In addition, these landmarks are not generally the objects of interest in screening mammograms; at best they serve as intermediates toward registration and subsequent detection or characterization of anomalies associated with disease. Thus conclusions regarding the disease state of tissue requires first the accurate detection of the landmarks, then correct registration and finally correct detection of the anomalies of interest.

This paper reports a key step in replacing registration of mammograms based on general landmarks by registration of the objects of interest themselves. Specifically, the goal is to segment mass-like regions in the mammogram for the future purpose of studying the

978-0-7695-3866-2/09 $26.00 © 2009 IEEE
DOI 10.1109/DICTA.2009.72

similarity and differences between mass-like objects in different views (say from different screening visits) of the same breast. This context is important for formulating the exact objective of the segmentation and for evaluating the performance.

Numerous algorithms have appeared for automatic detection of masses in screening mammorgrams. Generally, the steps are to find the boundary of the anomaly as accurately as possible, measure shape, size, contrast, and texture features within the anomaly, around the anomaly or on the border and classify the objects as a mass or non-mass or as a malignant or benign mass. For these schemes, the boundary must be such as to maximally capture differences in the measured features inside and outside (or on the border of) the anomaly. Normally, an assumption is made that such a boundary coincides with the visually apparent boundary.

In contrast, the objective here is to identify objects that could possibly be masses and identify the general shape, size, contrast, location, ect. only. The exact boundary is not needed and is not even desirable since the appearance of the object in another view of the same breast may not be the same. For this reason, the performance of the segmentation should not be measured by comparing boundaries of objects with "true" boundaries drawn by an expert. The ultimate measure of segmentation performance is the ability of the final scheme to detect breast cancer, but this is an unrealizable criterion during the development stage. The approach taken here is to compare segmented regions with general information of anomalies provided by an expert. Instead of a carefully drawn boundary, the expert information consists of a centerpoint indicating the location of the anomaly and a circle or a box that roughly indicates the size.

The segmentation method used is a graph-theory method based on minimum spanning trees (MST) [2]. MST segmentation is attractive in this setting for a number of reasons. First, methods based on graphs are able to combine both global and local image information in the segementation process and, among graph based methods, the MST is fairly fast. Second, previous work indicates that this method is quite robust to shifts, rotations and warping of the type expected when comparing sequential screening mammograms [8]. Third, applying the MST algorithm requires choosing only one parameter. This is a distinct advantage over methods that rely on a larger collection of parameters that must be chosen at hoc for each class of images or for each individual image. The single parameter needed to run MST is denoted by $k$ and controls the granularity of the resulting segmentation [2], [9]. Because $k$ has a predictable effect on the nature of the segmentation, it can be used to tune the process optimaly. This approach was used in [15] to detect optimal accurate boundaries of the pectoral muscle line in mammograms using the image entropy measure introduced in [18].

In the present work, the granularity parameter, $k$, is used to optimize the MST algorithm for the purpose of identifying mass-like regions. The motivation for this approach comes from the variety of breasts encountered in screening mammography. Some breasts appear in mammograms as essentially featureless with little dense tissue and very few features which could be interpreted as mass-like. Other images, sometimes called "busy breasts", comprise a variety of intensity variation and many mass-like regions. In each case, better segmentation results if a good ballance is achieved between the use of overall variation of image intensity and local variation associated with mass-like regions. This motivates measuring the criterion for optimal segmentation as a balance between overall and local image entropy as in [15] and [18].

Since MST segmentation is very sensitive to noise, a denoising filter has to be used before the segmentation process is performed. In what follows this problem is addressed in depth by quantifying the results of segmentation after preprocessing by a gausian filter (most often used in the literature for MST segmentation), an anistropic filter ([11]), and a very new, neutrosophic denoising method ([4]).

## 2 MST segmentation

The MST segmentation method was proposed in [2] and was adapted for mammography in [9]. The key structures needed for the present application are as follows.

Let $G = (V, E)$ be an undirected graph where, $V$, the set of vertices, is taken to be the set of pixels that form the image and $E$ is a set of edges that connect neighboring pixels. Elements of $E$ are denoted by $(v_i, v_j)$ where $v_i$ and $v_j$ are elements of $V$. Every pair of vertices is assigned a weight, $w$, by

$$w\left((v_i, v_j)\right) = \begin{cases} \left|I(v_i) - I(v_j)\right|, & (v_i, v_j) \in E, \\ \infty, & \text{otherwise}, \end{cases}$$

where $I\left(v_i\right)$ is the image intensity at $v_i$. A component of $G$ is a graph $C = (V', E')$, where $V' \subset V$ and $E' \subset E$ and with the property that for every pair of vertices in $V'$ there exists a sequence of edges in $E'$ such that the catenation of the sequence connects the two vertices. A tree that spans a component $C$ and has a minimum total weight is called a *minimum spanning*

*tree* of $C$ (MST($C$)). A segmentation of $G$ is a collection of components $C_k = (V_k, E_k)$ such that $\cup V_k = V$ and $V_i \cap V_j = \emptyset$ for $i \neq j$.

For a component $C \in G$ and minimum spanning tree MST($C$), the *internal difference*, $Int(C)$, is defined as the largest weight in MST($C$). For two components $C_1$ and $C_2$, their difference $Diff(C_1, C_2)$ is defined as the minimum weight connecting $C_1$ and $C_2$.

The MST algorithm builds a new graph $H = (V, F)$. Initially, $F = F_0$ is the empty set, meaning that each vertex (pixel) is a component unto itself. In subsequent iterations, components $C_1$ and $C_2$ are merged, meaning that $C_1$ and $C_2$ form a single component, if

$$Diff(C_1, C_2) \leq \min\left(Int(C_1) + \tau(C_1), Int(C_2) + \tau(C_2)\right),$$

where the threshold function $\tau$ is given by $\tau(C) = \frac{k}{|C|}$, $|C|$ denotes the number of elements in $C$, and $k$ is a constant. The process terminates when no new mergers are allowed.

The constant $k$ controls the granularity and hence the quality of the segmentation. Even very close values of $k$ may produce very different segmentations, as the Figure 1 shows. In most applications of the MST algorithm, $k$ is fixed empirically for a class of images with the result that the granularity is far from optimal for some members of the class. In this paper, $k$ is adjusted automatically for each image by optimizing the measure of entropy described in the next section.

## 3 Entropy of a segmentation

The following function of an image $I$, was proposed in [18] as a measure of effectiveness of an image segmentation:

$$H(I) = H_l(I) + H_r(I). \quad (1)$$

The first term - the *layout entropy* - measures the global image disorder (generally it increases with the number of components), and is defined by the formula

$$H_l(I) = -\sum_{j=1}^{N} \frac{|C_j|}{|I|} \log \frac{|C_j|}{|I|},$$

where $|I|$ is the area of the whole image and $|C_j|$ is the area of the $j$-th component.

The second term - the *region entropy* - measures the uniformity within components (it decreases when the number of regions increases), and is given by the formula

$$H_r(I) = \sum_{j=1}^{N} \frac{|C_j|}{|I|} H_\mu(C_j),$$

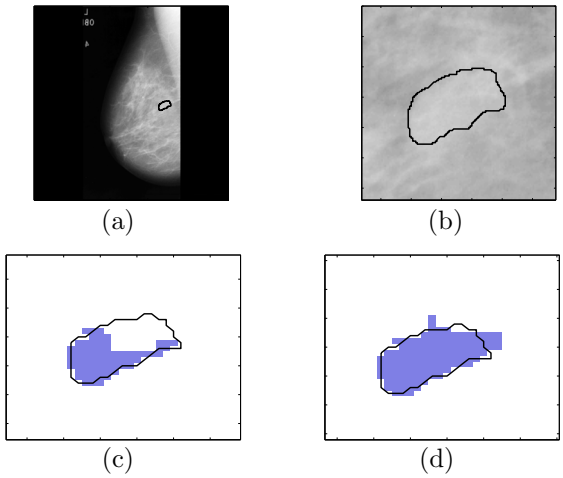


**Figure 1. Granularity of a segmentation. (a) The original mammogram (mdb091 from Mini-MIAS database) showing the location of the mass. (b) The contour zoomed. (c) The segmented mass for $k = 28$. (d) The segmented mass for $k = 29$.**

where $H_\mu(C_j)$ is the entropy of attribute $\mu$ for component $C_j$. In [18], luminance was used as the attribute $\mu$. In this paper, $\mu$ is the image intensity value of the pixel. Denoting by $M_j$ the set of values associated with feature $\mu$ in component $C_j$ and by $L_j(m)$ the number of pixels in component $C_j$ with value $m$ for feature $\mu$, the entropy of component $C_j$ is expressed as

$$H_\mu(C_j) = -\sum_{m \in M_j} \frac{L_j(m)}{|C_j|} \log \frac{L_j(m)}{|C_j|}.$$

## 4 Neutrosophic image denoising

The concept of neutrosophic image denoising was introduced in [3] and successfully applied to segmentation of natural and synthetic images in [4]. In [3] the neutrosophic filter (NS filter) was proposed for image denoising and a comparison with the median and mean filter was reported. The NS filter outperformed the other filters when applied to images with different kinds and levels of noise.

For convenience we briefly describe NS filtering. An image $P$ is converted into its neutrosophic form by transforming each pixel $P(i, j)$ into its neutrosophic equivalent $P_{NS}(i, j) = \{T(i, j), I(i, j), F(i, j)\}$, where the coordinates indicate probabilities of the pixel membership in a region; $T$ % true, $I$ % indeterminate and

$F\,\%$ false. The membership values are defined as

$$\begin{aligned} T(i,j) &= \frac{\bar{g}(i,j) - \bar{g}_{min}}{\bar{g}_{max} - \bar{g}_{min}}, \\ I(i,j) &= \frac{\delta(i,j) - \delta_{min}}{\delta_{max} - \delta_{min}}, \\ \delta(i,j) &= |g(i,j) - \bar{g}(i,j)|, \\ F(i,j) &= 1 - T(i,j), \end{aligned}$$

where $g(i,j)$ is the intensity value of $P(i,j)$, $\bar{g}(i,j)$ is the local mean value of $g(i,j)$. The local $max/min$ values for $g$ and $\delta$ are calculated for symmetric neighbourhoods of $(i,j)$ with radius $w$.

The $\alpha$-filtering operation $\hat{P}_{NS}$ is defined on $P_{NS}$ as follows:

$$\hat{P}_{NS}(\alpha) = P(\hat{T}(\alpha), \hat{I}(\alpha), \hat{F}(\alpha)),$$

where

$$\begin{aligned} \widehat{T}(\alpha) &= \begin{cases} T, & I < \alpha \\ \widehat{T}_\alpha, & I \geq \alpha \end{cases}, \\ \widehat{T}_\alpha(i,j) &= \frac{1}{w \times w} \sum_{m=i-w/2}^{i+w/2} \sum_{n=j-w/2}^{j+w/2} T(m,n), \\ \widehat{I}_\alpha(i,j) &= \frac{\widehat{\delta}_T(i,j) - \widehat{\delta}_{T\,min}}{\widehat{\delta}_{T\,max} - \widehat{\delta}_{T\,min}}, \\ \widehat{\delta}_T(i,j) &= |\widehat{T}(i,j) - \widehat{\widehat{T}}(i,j)|, \\ \widehat{\widehat{T}}_\alpha(i,j) &= \frac{1}{w \times w} \sum_{m=i-w/2}^{i+w/2} \sum_{n=j-w/2}^{j+w/2} \widehat{T}_\alpha(m,n). \end{aligned}$$

The $\alpha$-filtering is performed on the image until the relative entropy of the indeterminate set $I$ is smaller than a specified threshold. In this study we used $\alpha = 0.85$ for all images, $w = 4$, for Mini-MIAS images, and $w = 6$ for our local database. The entropy thresholds were set to $10^{-3}$ and $5 \times 10^{-6}$ for Mini-MIAS and the local set, respectively. These values were determined empirically.

## 5 Databases

Two mammographic databases were used to test the method: the publicly available and widely used Mini-MIAS mammographic database [14], and a local database of mammograms.

The spatial resolution of Mini-MIAS images is 200 $\mu$m per pixel and the depth resolution is 8 bit. All images in the database are of 1024x1024 pixels in size. To reduce the computation time the images were subsampled by a factor of four to 256x256 pixels. Thus the final pixel size for the images used in experiments was 800 $\mu$m.

Mammograms from the local database were digitized at 50 $\mu$m per pixel and 12 bit depth resolution. The images were subsampled by the factor of 8, so that the final pixels size was 400 $\mu$m.

A set of 55 mammograms was selected from the Mini-MIAS database and another set of 37 mammograms was taken from the local database. The only criterion for selection was that at least one mass-like object was present and annotated by a radiologist with expertise in mammography.

## 6 Method

### 6.1 Mass coverage ratio

The ultimate goal of this study is to provide a rigorous method of selecting automatically $k$ value which results in a usable segmentation of all mass regions. Depending on the application 'usable' may be as little as $40\,\%$ of the mass area segmented properly, if only detection is concerned, or 70% or more if also classification is involved. However, it is critical that no mass-like object is missed, so the emphasis is more on being able to obtain a minimum coverage of masses than being able to segment accurately most mass-like objects but totally missing some of them. To meet this goal an appropriate measure of the segmentation quality is necessary.

We adopt measure $\mathcal{R}$ called the mass coverage ratio ([7]). $\mathcal{R}$ was computed for each mass-like region and each segmentation. Since an exact representation of the mass-like region is not necessary and not even possible due to undefined boundaries for masses, the subsequent processing includes the merging of components if, in aggregate, they are more mass-like. Accordingly, a suitable criterion for measuring the quality of the segmentation of mass-like regions is to compute how well the union of all reasonable components which overlap the annotated region fits the annotation. By a reasonable component is meant a component with at least half of its area residing within the annotated region. Thus a component $C$ is said to overlap the annotated region $T$ if

$$|C \cap T| > |C \setminus T|.$$

The mass coverage ratio is then defined by

$$\mathcal{R} = \frac{|A \cap T|}{|A \cup T|}, \tag{2}$$

where $A = \cup C_i$ and the union is taken over components that overlap $T$.

Since the MST segmentation parameter $k$ roughly determines the area of the smallest component in terms of numbers of pixels that can be retained, and circular objects having 3-5mm diameter are most important mass candidates the appropriate range of $k$ values can be estimated based on the spatial resolution of images. For Mini-MIAS mammograms, those objects have estimated area 27-34 pixels, while for images from our local database the area ranges from 110-134 pixels. Hence, the reasonable ranges for $k$ were estimated as 27-34, for Mini-MIAS mammograms and 110-134, for mammograms from the local database.

### 6.2 Noise reduction

Three methods for noise reduction were tested for use prior to MST segmentation. An anisotropic filter (see e.g. [11]), the symmetric Gaussian filter of size 6 (4 for Mini-MIAS images) with standard deviation $\sigma = 0.8$, and the neutrosophic filter described in Section 4. Figure 2 shows the range of mass coverage ratio for each mass in each database, obtained by varying $k$, after anistropic, gaussian and neutrosophic filtering.

Regardless of the kind of filter applied, one cannot generally expect that there is a single value of $k$ producing high $\mathcal{R}$ values for each image. The local set of mammograms used in this study is an example of a collection where no such value exists. Gaussian and neutrosophic smoothing prior to segmentation reduced the range of $\mathcal{R}$ values substantially while anistropic filtering reduced the range less. The graphs also show that for each image there exist values of $k$ resulting in mass coverage ratio value of 40 % or higher. This observation motivated the search for an automatic method for chosing an optimal value of $k$ (in that it avoids disastrous mass coverage ratios) for each image.

### 6.3 Optimizing MST

To determine optimal values of the parameter $k$ the following algorithm was followed. Every mammogram was segmented for the specified range of values of $k$ as determined in Sec. 6.1. For each value of $k$, the entropy of the segmentation was computed using the formula in (1). The value of $k$ resulting in the smallest entropy segmentation was selected as an optimal one.

In order to be able to quantify the results, approximate mass contours were drawn (within the radiologist annotated areas) for each image. A single contour was used for each Mini-MIAS image (drawn by one of the authors), while for the more challenging local set

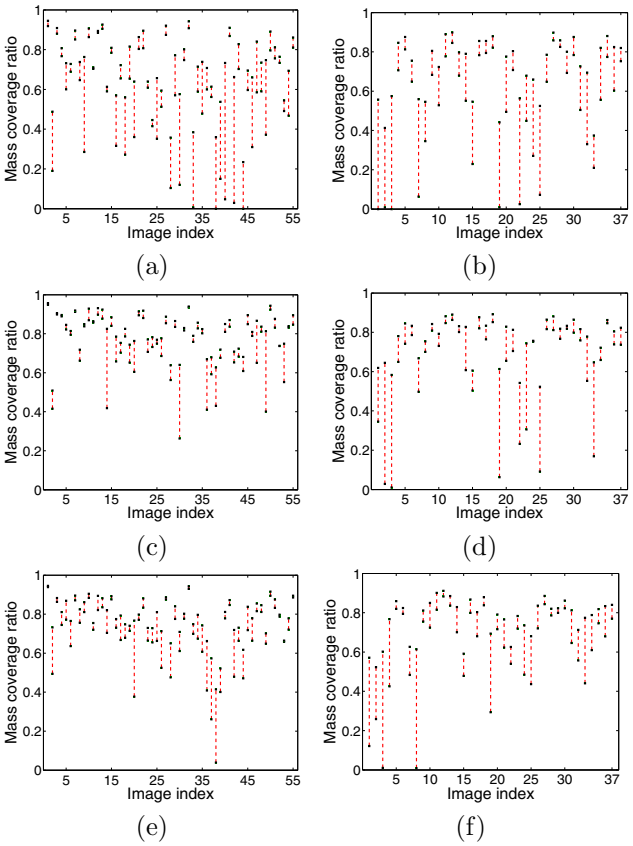


**Figure 2. For each image index, the vertical line segment indicates the range of $\mathcal{R}$ values obtained by various choices of $k$. (a), (c), (e) relate to Mini-MIAS images filtered with anistropic, gaussian and neutrosophic filters, respectively. (b), (d), (f) relate to local images filtered with anistropic, gaussian and neutrosophic filters, respectively.**

of images two contours were drawn independently by the authors, and both union and intersection of those contours were tested. This compensates for subjective estimation of boundaries of difficult to draw contours.

ImageJ software package ([12]) was used to annotate the images by the radiologist and to draw contours.

## 7 Results

Table 1 shows that all Mini-MIAS images were segmented successfully, that is, with $\mathcal{R}$ at least 40 %, when neutrosophic filtering was applied. Moreover, 69 % of images were segmented with a very high ratio (at least 70 %). For gaussian filtering the numbers are comparable while for the anistropic filtering they are signifi-

**Table 1. Mass coverage ratio by range for the Mini-MIAS set for each of the three filters. The first number gives the number of images falling into that range for some values of $k$. The corresponding number for $k$ value selected with our method (the optimal value) is shown in brackets. Local database images were tested for the union and intersection of two contours drawn by the authors according to the radiologist annotations.**

| Mini-MIAS set | | | |
|---|---|---|---|
| filter | less than 40% | [40-70)% | 70%+ |
| anisotropic | 16 (8) | 19 (24) | 20 (23) |
| gaussian | 1 (1) | 18 (16) | 36 (38) |
| neutrosophic | 3 (0) | 21 (17) | 31 (38) |
| **Local set with union of contours** | | | |
| filter | less than 40% | [40-70)% | 70%+ |
| anisotropic | 12 (8) | 12 (9) | 13 (20) |
| gaussian | 8 (6) | 7 (7) | 22 (24) |
| neutrosophic | 5 (3) | 13 (9) | 19 (25) |
| **Local set with intersection of contours** | | | |
| filter | less than 40% | [40-70)% | 70%+ |
| anisotropic | 15 (11) | 11 (7) | 11 (19) |
| gaussian | 9 (7) | 12 (12) | 16 (18) |
| neutrosophic | 11 (6) | 16 (11) | 10 (20) |

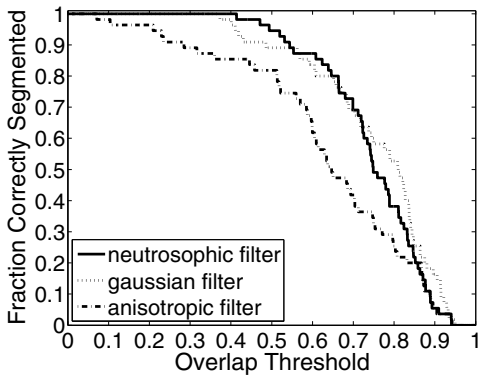


**Figure 3. The performance of MST segmentation for the three filters on the Mini-MIAS set.**

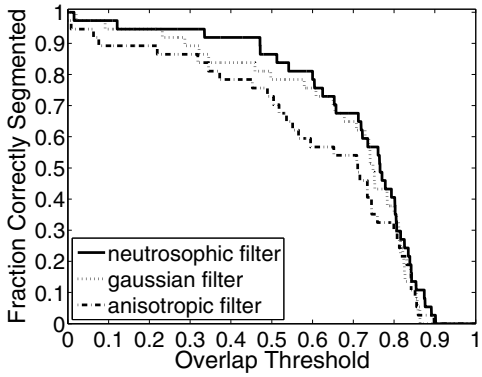


**Figure 4. The performance of MST segmentation for the three filters on the local data set for union of contours.**

cantly worse.

For images from our local database the ratios were obtained for both union and intersection of two independently drawn contours by the authors, according to the radiologist annotations. These are shown separately in Table 1. In all cases the superiority of neutrosophic filtering is visible. It allowed for about 50 % reduction of number of potential failures (those less than 40 % segmented). The results for the gaussian filtering were comparable, while the anistropic filtering produced significantly worse outcomes.

Figures 3, 4 and 5 show plots of the proportion of correctly segmented masses as functions of the overlap threshold used to define successful segmentation for various versions of segmentation methods discussed. The graphs indicate that the performances of MST segmentation for gaussian and neutrosophic filters are comparable and outperform the segmentation for images with anisotropic filtering.

Looking at the details of ratio values on image-by-image base, Figures 7, 6 we also conclude that the anistropic filtering is not appropriate for MST segmentation and the neutrosophic one outperforms both the gaussian and anistropic filtering in terms of minimizing the number of failures (images with less than 40 % segmentation ratios).

Comparing Figures 3, 4 and 5 to the one obtained in [7] (indicative only since different databases were used) we see that MST segmentation is capable of producing radiologist-like outlines.

## 8 Discussion

There were two images (out of 37), in our local database set, where (regardless of the filter used) the method did not work. That is, in those cases the optimal mass coverage ratio was smaller than 40 % both

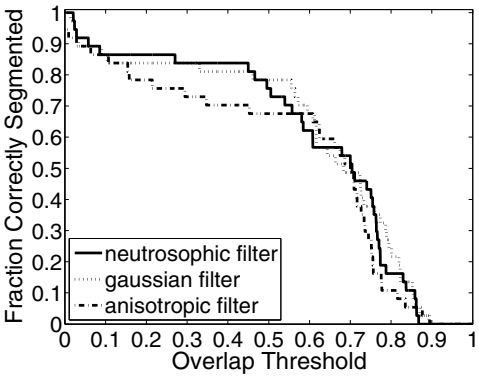


**Figure 5. The performance of MST segmentation for the three filters on the local data set for intersection of contours.**

for the union and intersection of contours.

Figure 8 shows the images annotated by a radiologist together with their optimal segmentation. It is evident from the images that the mass is hardly visible in the first case, and is literally invisible in the second. In both cases the boundaries are extremely hard to detect. Very low saliency of the objects resulted in oversegmentations for most values of $k$. Since the entropy method favors the segmentation in which a few segments dominate (similarly to human perception) (this was recently proved rigourously in [17]) it assigned the best score to an oversegmented image partition, (shown in Figure 8 (c), (d)).

## 9 Conclusion and further work

The study shows that automatic tuning of MST segmentation by using a measure of entropy to select one of several possible segmentations has a potential to deliver useful delineation of mass-like objects in mammograms for the purpose of CAD systems. It is capable of producing very high mass coverage ratio for majority of mammograms and, more importantly, producing very few failures. This is a critical issue, since the outcome of the segmentation will become an input into CAD and mammogram registration methods. A disadvantage of the proposed method is that every image must be segmented several times before the best segmentation can be selected.

It is expected that for some applications the obtained approximate contours will be subject of further processing using one of the numerous region-merging algorithms available in literature (e.g. [13] or [5], [1]) and active contour models (e.g. [6], [16]) to futher improve their accuracy before being used for detection

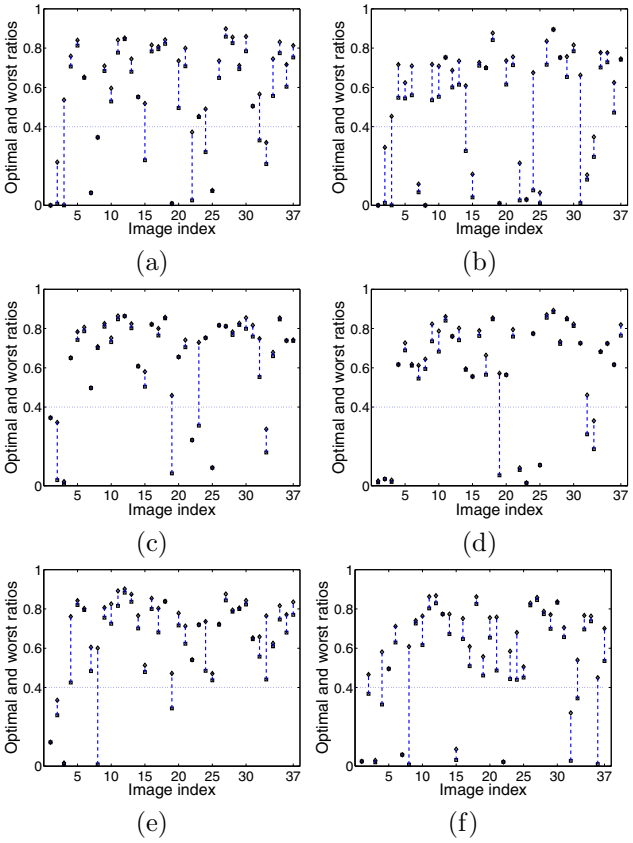


**Figure 6. Comparison of $\mathcal{R}$ values for the local set. (a), (c), (e) For union of contours for the anisotropic, gaussian and the neutrosophic filter, respectively. (b), (d), (f) For intersection of contours for the anisotropic, gaussian and the neutrosophic filter, respectively. For each image index, the vertical line segment connects the worst and the optimal ratio values.**

algorithms.

## References

[1] J. Cousty, M. Couprie, N. L., and G. Bertrand. Weighted fusion graphs: Merging properties and watersheds. *Discrete Applied Mathematics*, 156:3011–3027, 2008.

[2] P. F. Felzenszwalb and D. P. Huttenlocher. Efficient graph-based image segmentation. *Int. J. Comput. Vision*, 59(2):167–181, 2004.

[3] Y. Guo, H. Cheng, Y. Zhang, and W. Zhao. A new neutrosophic approach to image denoising. In *Proceedings of the 11th Joint Conference on Information Science*, pages 1–6. Atlantis Press, 2008.

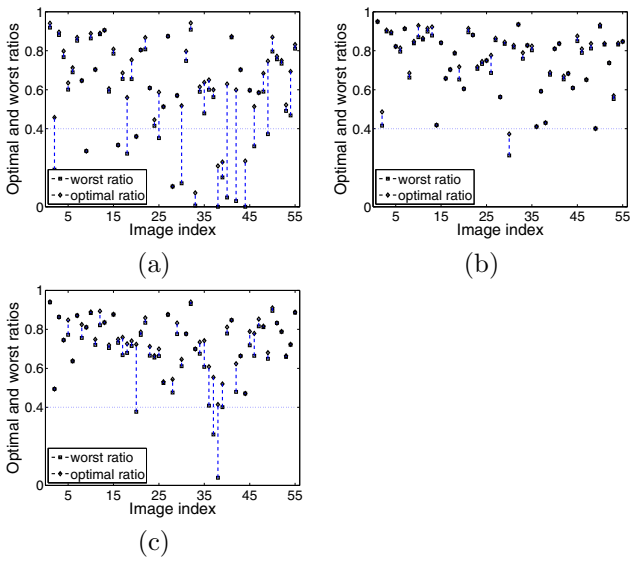


**Figure 7. Comparison of $\mathcal{R}$ values for the Mini-MIAS set. (a) For the anisotropic filter, (b) for the gaussian filter, (c) for the neutrosophic filter.**

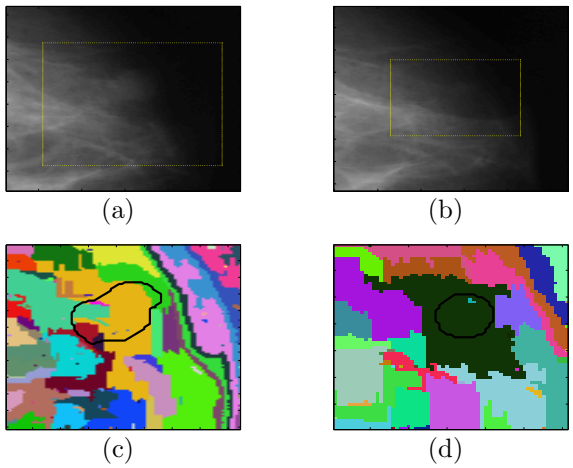


**Figure 8. Two difficult cases from the local database. (a), (b) Zoomed annotation areas. (c), (d) Optimal segmentations found.**


[4] Y. Guo and H. D. Cheng. New neutrosophic approach to image segmentation. *Pattern Recognition*, 42:587–595, 2009.

[5] K. Haris, S. N. Efstratiadis, N. Maglaveras, and A. K. Katsaggelos. Hybrid image segmentation using watersheds and fast region merging. *IEEE transactions on Image Processing*, 7:1684–1699, 1998.

[6] M. Kass, A. Witkin, and D. Terzopoulos. Snakes: active contour models. *Int. J. Comput. Vision*, 1(4):321–331, 1987.

[7] M. Kupinski and M. L. Giger. Automated seeded lession segmentation on digital mammograms. *IEEE Transactions on Medical Imaging*, 17(4):510–517, 1998.

[8] F. Ma, M. Bajger, and M. J. Bottema. Robustness of two methods for segmenting salient features in screening mammograms. In *Proc. of the 9th Conf. on Digital Image Computing Techniques and Applications (DICTA2007)*, pages 112–117, Adelaide, 2007.

[9] F. Ma, M. Bajger, J. P. Slavotinek, and M. J. Bottema. Two graph theory based image segmentation methods for identifying pectoral muscle in mammograms. *Pattern Recognition*, 40:2592–2602, 2007.

[10] K. Marias, C. Behrenbruch, S. Parbhoo, A. Seifalian, and M. Brady. A registration framework for the comparison of mammogram sequences. *IEEE Trans. on Medical Imaging*, 24(6):782–790, June 2005.

[11] P. Perona and J. Malik. Scale-space and edge detection using anisotropic diffusion. *IEEE Pattern Anal. Machine Intell.*, 12:629–639, 1990.

[12] W. S. Rasband. *ImageJ*. U.S. National Institutes of Health, Bethesda, Maryland, USA, http://rsb.info.nih.gov./ij/, 1997-2008.

[13] M. Sonka, V. Hlavac, and R. Boyle. *Image processing, Analysis, and Machine Vision*. Thomson, 3 edition, 2008.

[14] J. Suckling, J. Parker, D. Dance, S. Astley, I. Hutt, C. Boggis, I. Ricketts, E. Stamatakis, N. Cerneaz, S. Kok, P. Taylor, D. Betal, and J. Savage. The mammographic images analysis society digital mammogram database. *Exerpta Medica*, 1069:375–378, 1994.

[15] H. Susukida, F. Ma, and M. Bajger. Automatic tuning of a graph-based image segmentation method for digital mammography applications. In *Proc. of the 5th IEEE Intern. Symp. on Biomedical Imaging (ISBI 2008)*, pages 89–92, Paris, France, May 14-17 2008.

[16] C. Xu and J. L. Prince. Snakes, shapes, and gradient vector flow. *IEEE Transactions on Image Processing*, 7(3):359–369, 1998.

[17] H. Zhang, J. E. Frits, and S. A. Goldman. Image segmentation evaluation: A survey of unsupervised methods. *Computer Vision and Image Understanding*, 110:260–280, 2008.

[18] H. Zhang, J. E. Fritts, and S. A. Goldman. An entropy-based objective evaluation method for image segmentation. In *Proc. of SPIE: Storage and Retrieval Methods and Applications for Multimedia*, volume 5307, pages 38–49, 2004.